

December 5, 2021

EAS 4580

Volatiles and Volcanism: Analyzing Iki Melt Inclusions for Carbon Dioxide, Water, and Carbonate Content

Researcher: Auden Reid-McLaughlin

Supervisor: Charlotte Devitre

1. Introduction

A main controlling factor on the explosivity of an eruption is the dissolved volatile content, such as carbon dioxide and water. Once the melt becomes supersaturated in volatiles, the gases exsolve from the magma by nucleating bubbles. The exsolution of low density gases drives volcanic eruptions, as the bubbles coalesce and degass, driving the magma upwards due to the pressure created in the conduit. Further, water in particular controls physical and chemical characteristics of the magma such as crystallization and polymerization, and therefore affects physical properties of the magma such as density and viscosity, which in turn influence eruptive behavior. Therefore, measuring the volatile content of the source magma allows researchers to better understand the behavior of the eruption in terms of its explosivity. Secondly, measuring the volatile content in the initial magma source allows us to constrain the depth of the source, and therefore construct a fuller picture of the plumbing system for the given volcano.

But how do we measure the initial volatile content if the erupted material has been degassed, as happens during the ascension of the magma? Melt inclusions are pockets of initial melt that have been trapped inside crystals that formed at depth that act like pressure vessels. Melt inclusions contain the dissolved volatiles in the magma at the pressure, and therefore depth at which they were trapped, and ideally, the crystal protects the melt from further modification. Therefore, measurement of the total volatile content in the melt inclusion allows us to make such calculations. I emphasize total volatile content here, as we have to measure not only the content in the melt, but in the vapor bubble as well. The vapor bubble forms with cooling and decompression, where the melt contracts and the void space is filled by volatiles that are no longer soluble in the melt.

I spent my semester looking for and analyzing melt inclusions in olivine from the Kilauea Iki Eruption in 1959. In addition to the detection of pure CO₂ and water, a main driver behind this project was to identify inclusions with carbonate content in and around the vapor bubble as well as carbon dioxide in the bubble. Research up until now involving Iki samples has only looked at the vapor phases of CO₂ in melt inclusions (both in glass and vapor bubble), when in actuality, vapor bubbles host a variety of solid phases as well, including carbonates. Studies have shown that up to 80 percent of CO₂ that is 'lost' from the

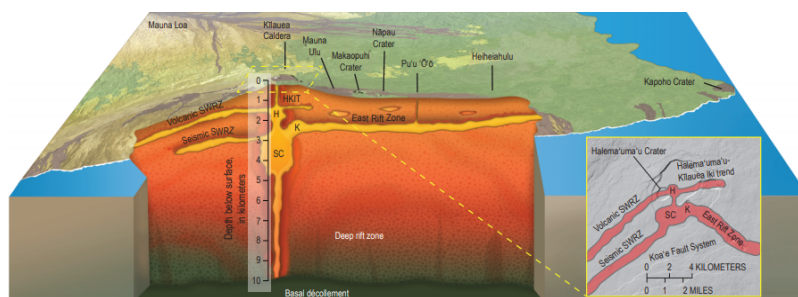
glass during vapor bubble formation can be hosted in the solid carbonate phases that form in the vapor bubbles as CO₂ concentrates (Venugopal et al. 2020), but this possibly significant carbon reservoir has not been included in melt inclusion analysis. This could potentially lead to underreporting of actual CO₂ initially present in magma. I was hoping to identify melt inclusions with both carbonate and CO₂ that would be suitable to run a homogenization experiment, where the carbonate is heated and converted into carbon dioxide to be re analyzed for CO₂ content, to get a more accurate concentration.

My project was focused on the first stage of constraining initial volatile content, where I mainly worked on picking melt inclusions, polishing and mounting them, running Raman analysis, then doing post analysis to find the CO₂ content in the vapor bubbles.

2. Background

Kilauea sits on the southeastern flank of Mauna Loa in Hawai'i, which for many years led scientists to believe that they shared a plumbing system. However, over the past few decades, it has been shown that it has its own plumbing system that extends from the surface deeper than 60 kilometers, where it then connects to the hotspot mantle plume which is the shared magma source for the Hawaiian Island chain. Kilauea shares this system with several other volcanic vents along the east rift zone, and it's also possible that Mauna Kea shares the magma source, though its near surface reservoir is much larger. Before Kilauea eruptions, most of the magma entering the volcano is stored temporarily within a shallow reservoir. The depths of the magma source are constrained by seismic activity due to the accumulation and upward movement of magma, and the shallower reservoirs have typically been constrained by measures of ground deformation. Figure 1 below shows a proposed structure of the plumbing system where several reservoirs correspond to different eruptive vents.

Kilauea has erupted dozens of times since 1952, with a near continuous eruptive behavior along the East rift zone from 1983 until the 2018 eruption. Figure 1b shows the lava flows from Kilauea since 1790, and as you can see, they pretty much cover the entire southeastern flank of the island. The volcano is actually currently erupting from a single vent on the western wall of summit crater, Halema'uma'u, and therefore a deeper understanding of the magma source is pertinent.



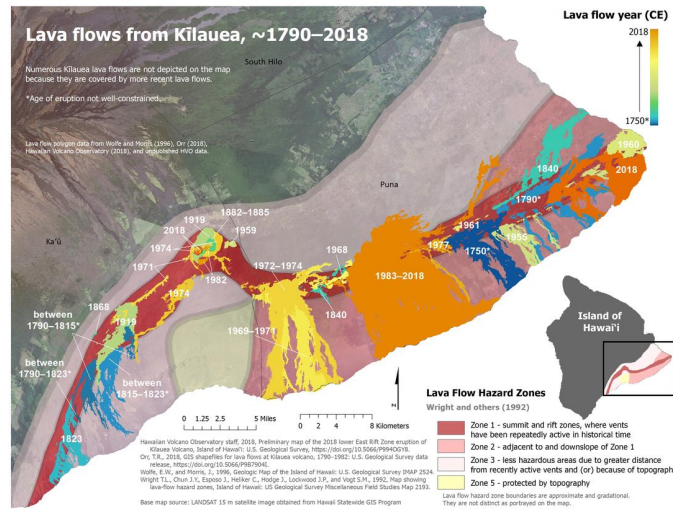


Figure 1: a) Proposed plumbing system underneath Kilauea and associated vents (USGS), b) Lava flows around Kilauea from 1790-2018 (USGS)

My research involves samples from the 1959 Kilauea Iki eruption. Iki refers to the pit crater directly next to the summit of Kilauea, shown in Figure 2a, along the Eastern Rift Zone of the Kilauea plumbing system. In 1959, the crater erupted in a short lived sequence that lasted from November 14th to December 20th, and produced some of the most incredible fire fountains recorded, as well as gave some of the first measurable data about the reservoir system. Earthquake swarms were detected for about three months before the eruption began, and tiltmeter data suggested that the reservoir was inflating with magma, which acted as strong precursors to the eruptive sequence. On the night of November 14th, a fissure of small lava fountains broke through the southern wall of the crater. Lava from the fountains cascaded down the summit slope and began to pool in the crater, before diminishing to a single vent.

The eruption took place over 17 episodes, which are quickly summarized in Figure 2b. The figure emphasizes the incredible order of magnitude of magma involved in the eruption sequence. The highest fire fountain was produced in episode 15, which erupted columns 580 m into the air, the highest recorded in Hawaiian history. In Episode 17, the vent was erupting as much as 1.85 million cubic meters of lava every hour on December 15th. The lava lake in Iki crater reached a maximum depth of 126 meters during episode 8.

The depth of the lake was mainly controlled by the elevation of the vent, where if it was above the surface of the lake, it filled significantly faster. If it was below, it had to blast through the surface to continue erupting, and therefore erupted more slowly. There were also several drainback events during

inter-eruptive episodes, where large slabs of lake crust were actually pulled down into the vent, causing a counterclockwise whirlpool in the lake. The vent shape changed as the eruption progressed, which in turn affected the column shape and size. The development of the fire fountains occurred over a matter of seconds at some points, meaning the area was extremely hazardous for the duration of the eruptive sequence.

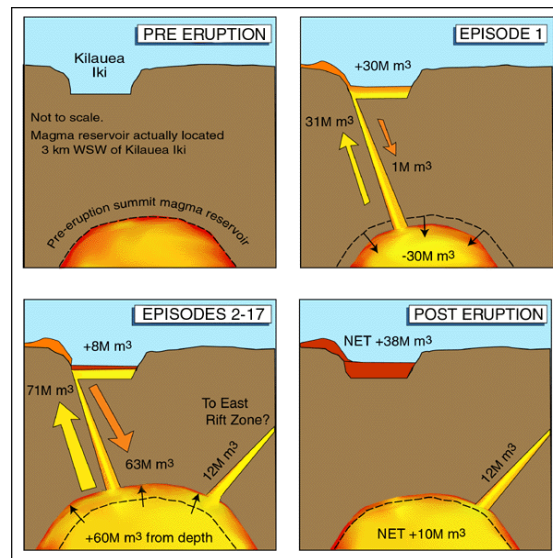


Figure 2: a) Geography of Kilauea and Iki Crater, b) Short summary of 1959 Iki eruptive sequence (USGS)

3. Materials and Methods

My project was split up into three separate components: picking the melt inclusions, running analysis for volatiles with Raman, and calculating the CO₂ content within the vapor bubbles.

3.1 Picking and Polishing

The majority of the project was spent picking melt inclusions that would be suitable for Raman. There are several obstacles with melt inclusion analysis, mainly involving degassing of the volatiles into the crystal and other erupted material as it ascends. However, some of these can be anticipated during the picking stage.

One of the main characteristics to look out for is decrepitation. Decrepitation refers to the rupture of the inclusion when internal pressure becomes too great, and therefore loss of volatiles to the surrounding crystal. This results in a characteristic pattern of very small, melt inclusion looking blebs near the main inclusion, a “tail” on the main inclusion, and/or circular striations in the crystal from the explosion of the bubble which can often be seen under the microscope, and are shown in Figure 3. The second characteristic is the presence of vapor bubbles. Since vapor bubbles represent the concentration of volatiles during decompression, it stands to reason that the presence of a vapor bubble can be indicative of a higher total volatile, and specifically CO₂ content in the inclusion. The third is the size of the inclusion. If an inclusion is large, it can indicate it has decrepitated. If the inclusion is small, it can indicate diffusion of water out of the inclusion, and therefore no longer representative of the initial volatile content of H₂O (Barth and Plank 2021). This diffusion is more likely to occur in small inclusions due to the higher surface area to volume ratio, which is conducive to higher rates of diffusion. The ideal range of inclusion size then falls between about 30 and 90 microns, though there are several inclusions smaller or larger that I identified.

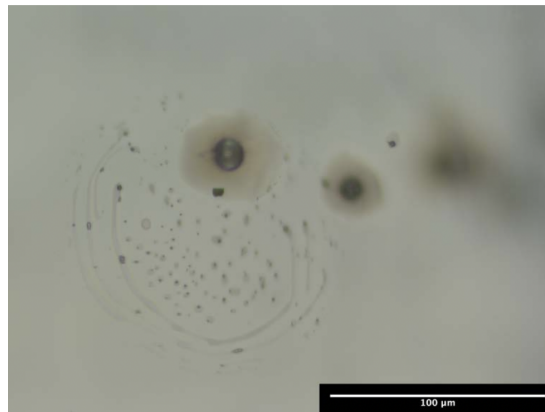


Figure 3: Example of decrepitated melt inclusion

After picking inclusions, the samples had to be prepped for Raman analysis. The samples had to be mounted on individual slides and polished so that the inclusions of interest were clearly visible under the microscope. This is important because during Raman, the vapor bubble edge must be clearly visible. Further, the top and bottom of the inclusion must be clear and visible during focusing so as to measure the thickness later on for the CO₂ calculation. The inclusions were crystal bonded to the slides, then polished first with 600 grit paper, then 800, then 1200 before finally polishing with aluminum powder to get the smoothest surface possible. This step could be very delicate where inclusions are close to the surface of the sample, as they cannot be exposed to the air since the volatiles will be completely lost.

3.2 Raman Analysis

After polishing the samples, they were ready for the Raman. The setup is shown in Figure 4a, where the microscope and laser are used in tandem during analysis. Raman is a type of spectroscopy that uses photon scattering known as Raman scattering to measure the vibrational modes of molecules within the sample. In short, the sensor measures the difference in energy of the laser photons before and after they hit the sample, which give information about the composition of the surface they are sampling and output a spectrum of intensity versus frequency. On the Raman spectra, carbon dioxide has a characteristic double peak around 1388 and 1286 which is called the Fermi diad shown in figure 4b, and the spacing between the two peaks is indicative of the density of CO₂ in the bubble. While the intensity cannot immediately tell the amount of CO₂ in the sample in ppm, it indicates whether or not CO₂ is present at all, as well as acts like a general indicator of relative amount. The spectrum also shows whether or not there is carbonate in the melt inclusion, with a peak around 1093, though this peak is much broader.

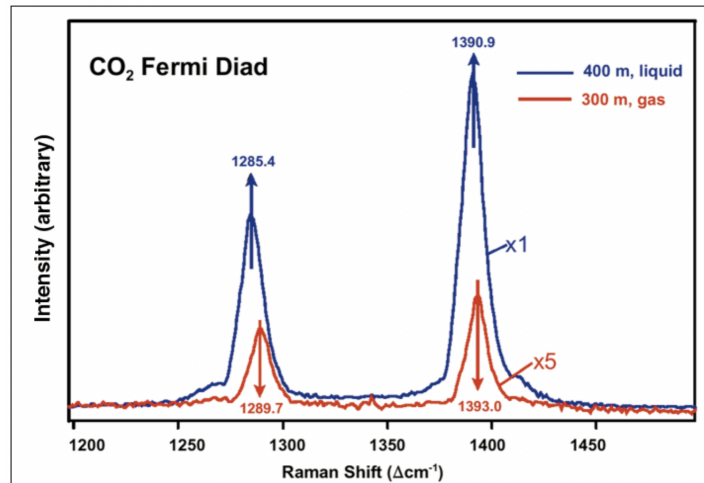
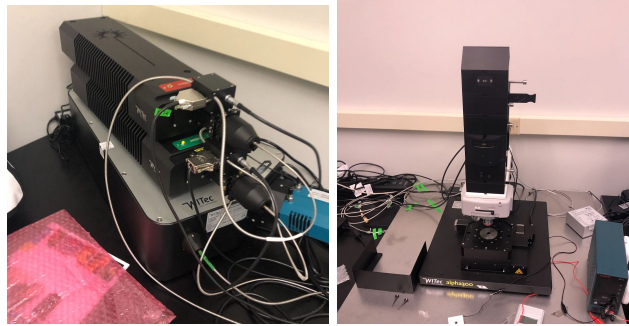


Figure 4: a) Laser and Microscope for Raman Spectroscopy in Snee Hall, Cornell University, b) Example Raman Spectra showing Fermi Diad (Pasteris et al. 2004)

For CO₂, analysis was run on 800 grating with a central peak at 1325. Initial acquisitions were run for 45 seconds, followed by 60 and 90 seconds if carbon dioxide was present. For water, analysis was run on 300

grating with a central peak at 2300. After line scan analysis to determine the most water dense depth within the inclusion, 3 acquisitions of 60 seconds were run.

3.2 CO2 Calculation

Once the spectra were gathered, the next step was to calculate the amount of CO2 in the vapor bubble. First, peaks were fitted to the carbon dioxide data in Fityk to determine the central frequencies. On the neon data, peaks to the right and left of the Fermi Diad were then found, which were normally around 1447 and 1116. Ratio of the observed neon peak separation with the actual separation was calculated, and then multiplied by the separation of the observed Fermi Diad in order to correct it. This corrected Fermi Diad was then used to determine the density of CO2 in the vapor bubble.

In order to calculate the CO2 content, geometry calculations of the melt inclusions had to be made. First, the thickness of the inclusions must be measured under the microscope. The inclusions then were measured in Fiji Image6, and were approximated as elliptical. The vapor bubbles were approximated as spherical. The volume of the inclusion and bubble were then calculated, along with the bubble fraction (i.e. the fraction of the volume of the inclusion taken up by the bubble). The amount of CO2 in the bubble can be calculated according Equation 1 below, where a density of 2.8 for glass is assumed, and f refers to the bubble fraction. This amount is converted from mL/cm^3 to ppm by a factor of 10^6 .

$$\Delta CO_{2(bubble)} = \frac{\rho_{CO2(bubble)} * f_{bubble}}{\rho_{glass} * (1 - f_{bubble})}$$

Equation 1: CO2 within vapor bubble equation

4. Results and Discussion

The results of the experiment are shown below. Of 49 inclusions identified across 23 samples throughout the semester, 4 were determined to contain CO2, and 1 was found to contain carbonate.

4.1 Raman Spectra

Figure 5a shows the 4 CO2 containing inclusions with measurements. Figure 5b shows the overlaid outputted Raman spectra of the 4 CO2 containing inclusions. The spectra have been plotted on the same axis (i.e. unnormalized). Figure 5c shows a cascading graph of all the spectra, where relative abundances are easier to spot.

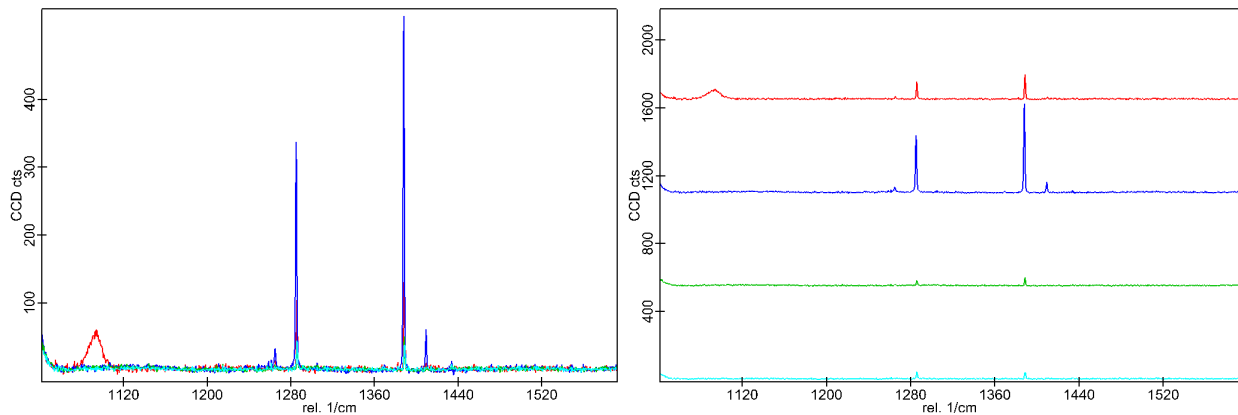
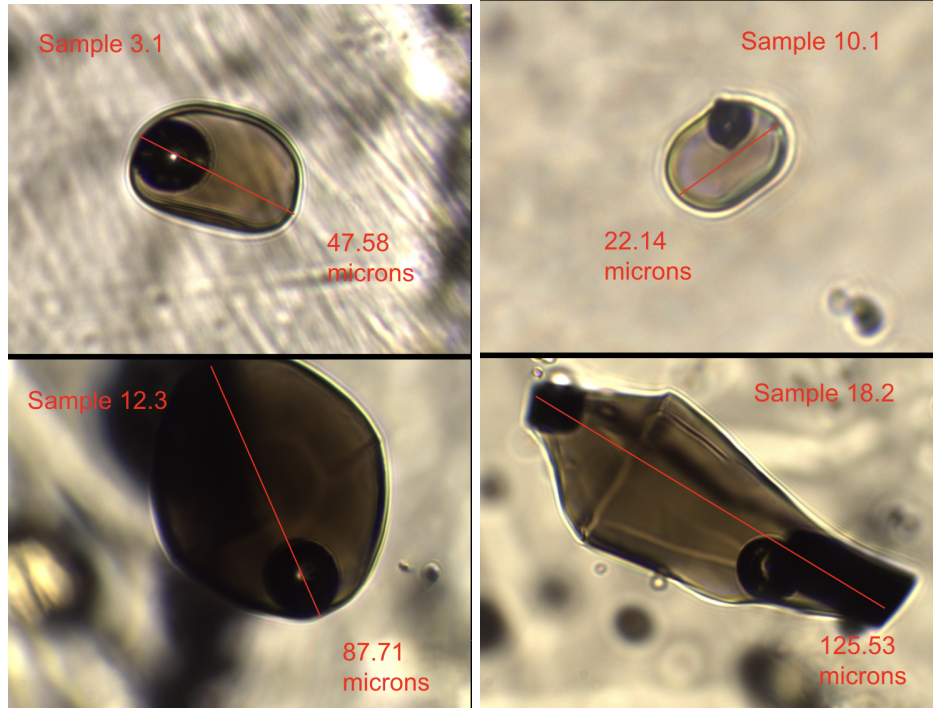


Figure 5: a) Inclusions identified containing carbon dioxide, b) Overlaid Raman Spectra of inclusions shown above, Legend: Dark Blue=3.1, Red=10.1, Green=18.2, Light Blue=12.3, c) Cascading plot of Raman Spectra, same legend

There are several key features to note in the spectra. First, relative abundances of carbon dioxide are clear in both Figure 5b and c. Sample 3.1 and 10.1 have a significantly higher intensity of the CO₂ peaks than samples 12.3 and 18.2. In Figure 5c, it is clear the samples 12.3 and 18.2 have comparatively very low CO₂, which illustrates the lack of CO₂ in the samples ran through Raman in general. The second feature of note is the carbonate peak in sample 10.1, which is not present in any of the other samples that include CO₂, nor is it present in any other inclusions analyzed. Figure 5c shows the intensity at this peak is comparable to the CO₂ intensity measured. This sample seems to also have the second most intense CO₂

spectrum, which could point to the carbonate as a potential reservoir for carbon from what has originally been CO₂ in the initial magma.

4.2 CO₂ Concentration

Table 1 shows the geometric information, CO₂ density and content broken down by sample. Figure 6 displays two functions, CO₂ content as a function of bubble volume and as a function of bubble fraction.

Inclusion #	Bubble Volume (cm ³)	Inclusion Volume (cm ³)	CO ₂ Density	Bubble Fraction	△CO ₂ in Bubble (ppm)
3.1	4.4548E-09	1.21286E-08	0.11532567	0.36730044	23910.6759
10.1	3.1323E-10	1.74506E-09	0.09872151	0.17949491	7713.023
12.3	8.2068E-09	3.39905E-07	0.09760476	0.02414435	862.467852
18.2	5.5041E-09	1.53837E-07	0.10092066	0.03577892	1337.43512

Table 1: Calculated features of Identified Inclusions

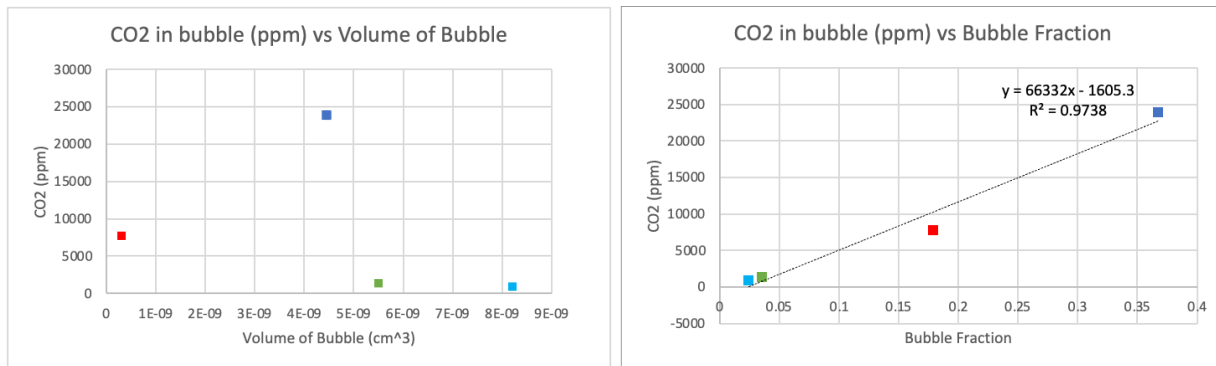


Figure 6: a) Plot of CO₂ concentration vs. Bubble Volume, b) Plot of CO₂ concentration vs. Bubble Fraction

From Figure 6a, there does not seem to be a clear correlation between CO₂ content in ppm and bubble volume. However, Figure 6b seems to show a very positive correlation between CO₂ content and bubble fraction, with an R² value of 0.973. Clearly, as the bubble fraction of the samples increases, the amount of CO₂ found in the bubble does as well. Regardless, there is very clearly a wide range of bubble volumes and bubble fractions found in these inclusions from Iki.

There are several possible explanations for this behavior. According to Allison et al. 2021, olivine samples from explosive basaltic eruptions at Sunset Crater, Arizona were analyzed and a similar range of

bubble volumes were found. Large bubble fractions can be attributed to several factors assuming they originated by shrinkage, including separate cooling history from smaller bubbled inclusions, H⁺ diffusion during pre-eruptive cooling, and post-entrapment cooling, where the latter is the mechanism determined by Allison. Post-entrapment cooling can lead to heterogeneous entrapment of melt inclusions as two separate phases, the liquid melt and exsolved, vapor CO₂ phase simultaneously. It is also possible that these larger bubbles are not from melt inclusion shrinkage, and originate from another source altogether, as discussed in Tucker et al. 2019, where anomalously large bubbles within melt inclusions were found to actually be indicators of fracturing of olivine phenocrysts, or trapping of magmatic bubbles during ascension. The latter mechanism indicates that the CO₂ present in the melt inclusion is from an already formed bubble at a later stage of the eruptive process further up the conduit, and in discussion with Professor Gazel, this is more commonly found in Plinian eruptions.

It is also important to point out how Sample 3.1 falls under the trendline on Figure 6b, indicating that it may be underreporting the amount of CO₂ in the bubble as it is the only inclusion that hosts carbonate.

5. Conclusions and Next Steps

Over the past semester, I have analyzed melt inclusions from the 1959 Kilauea Iki eruption to calculate volatile and carbonate content, from picking samples, to Raman analysis, to calculation of CO₂ concentration in the samples. I was able to identify four inclusions with CO₂ content, and one with carbonate content. Interestingly, a very wide range of bubble sizes and fractions were discovered in these inclusions. There appears to be a positive correlation between the vapor bubble fraction and the concentration of CO₂ in the bubble. Since there are only four points of data in this analysis, it is difficult to constrain the exact reason behind the variation in bubble size, but it can be split into possible mechanisms based on whether or not the bubble originated as a product of melt inclusion shrinkage, or outside the inclusion altogether.

There are several next steps for this project. The first would be to identify more inclusions from the eruption and repeat the process and analysis laid out in the paper to get a wider sample size from which to study the mechanisms behind the bubble formation. The second is to perform a homogenization experiment on the inclusion that contains carbonate, sample 10.1, as well as any other samples identified later on with carbonate content, when the inclusion would be heated to turn the carbonate back into the CO₂ vapor phase. The inclusion would then be re-analyzed with Raman to identify the change in CO₂ concentration. The third step is to analyze the water content measured during my project. Constraining water in melt inclusions not only helps explain explosivity and physical properties of magma, but can help constrain ascension rates from modeling of diffusion.

6. Acknowledgments

This project allowed me to not only gain laboratory experience, but explore a deeper interest in mechanisms behind volcanic eruptions from a geochemical standpoint using real data. I am very grateful to have been given the opportunity, and I would like to thank Professor Esteban Gazel. I would also like to thank Charlotte Devitre who supervised my project and trained me, as well as Kyle Dayton who acted as an invaluable resource over the course of the semester.

7. References (in the order they appear)

Venugopal, S., Schiavi, F., Moune, S. *et al.* Melt inclusion vapour bubbles: the hidden reservoir for major and volatile elements. *Sci Rep* 10, 9034 (2020). <https://doi.org/10.1038/s41598-020-65226-3>

Richter, D. H., Eaton, J. P., Murata, K. J., Ault, W. U., & Krivoy, H. L. (1970). *Chronological narrative of the 1959-60 eruption of Kilauea Volcano, Hawaii* (Professional Paper 537E). [doi:10.3133/pp537E](https://doi.org/10.3133/pp537E)

U.S. Geological Survey, 1959 Kilauea Iki Eruption, accessed Nov. 30, 2021 at

<https://www.usgs.gov/volcanoes/kilauea/1959-kilauea-iki-eruption>

Barth, Anna, and Terry Plank. “The Ins and Outs of Water in Olivine-Hosted Melt Inclusions: Hygrometer vs. Speedometer.” *Frontiers in Earth Science*, vol. 9, Frontiers Media SA, 8 June 2021. Crossref,

[doi:10.3389/feart.2021.614004](https://doi.org/10.3389/feart.2021.614004).

Pasteris JD, Wopenka B, Freeman JJ, Brewer PG, White SN, Peltzer ET, Malby GE. Raman spectroscopy in the deep ocean: successes and challenges. *Appl Spectrosc.* 2004 Jul;58(7):195A-208A.

<https://doi.org/10.1366/0003702041389319>. PMID: 15282037.

Allison, C.M., Roggensack, K. & Clarke, A.B. Highly explosive basaltic eruptions driven by CO₂ exsolution. *Nat Commun* 12, 217 (2021). <https://doi.org/10.1038/s41467-020-20354-2>

Jonathan M. Tucker, Erik H. Hauri, Aaron J. Pietruszka, Michael O. Garcia, Jared P. Marske, Frank A. Trusdell, “A high carbon content of the Hawaiian mantle from olivine-hosted melt inclusions”, *Geochimica et Cosmochimica Acta*, Volume 254, 2019, Pages 156-172, ISSN 0016-7037, <https://doi.org/10.1016/j.gca.2019.04.001>.